Since January 2020 Elsevier has created a COVID-19 resource centre with free information in English and Mandarin on the novel coronavirus COVID-19. The COVID-19 resource centre is hosted on Elsevier Connect, the company's public news and information website.

Computational and Theoretical Chemistry 1204 (2021) 113375

Contents lists available at ScienceDirect

Computational and Theoretical Chemistry

journal homepage: www.elsevier.com/locate/comptc

Preliminary investigation of drug impurities associated with the anti-influenza drug Favipiravir – An insilico approach

S. Anil Kumar *, B.L. Bhaskar

Department of Chemistry, Amrita School of Engineering, Bengaluru Amrita Vishwa Vidyapeetham, India

A B S T R A C T

The role of repurposed or modified antiviral drugs has become more significant during the current global pandemic of SARS Covid-19. In the present study, four structurally analogous impurity molecules of antiviral drug Favipiravir are selected for preliminary computational investigation for assessing the structure-activity relationship. The optimized geometry and the electronic structures of the compounds are computed using Density Functional Theory as a precursor to evaluating their physical, chemical and spectral properties. The frontier orbitals analysis is performed to obtain global reactivity parameters namely, the chemical potential, absolute electronegativity, global softness, global hardness, electrophilicity, etc. The natural Bond Orbital (NBO) analysis and Mulliken analysis provided an understanding of the charge-transfer interactions of molecules. The possibilities of intermolecular interactions of the drug systems with the receptors are also visualized using the electrostatic potential maps (MEP) derived from the DFT computations. The physiochemical properties are assessed computationally using SwissADME webtool to correlate the structural aspects of the compounds with their biological responses. Useful parameters namely flexibility, lipophilicity, size, polarity, solubility and saturation were also computed to evaluate the therapeutic activity or drug-likeness.

1. Introduction

Favipiravir (FVPR), chemically 6-fluoro-3-hydroxypyrazine-2-carboxamide, is an antiviral drug cleared for treating pandemic infections in 2014 [1]. It has demonstrated uses in treating viral infections like Ebola, Yellow fever, West Nile virus, Foot and Mouth disease, Rift-valley fever, etc. [2,3]. Viruses causing seasonal influenza like H1N1, H2N2, H3N2 [2] and influenza A (H5N1) were also found to be vulnerable against FVPR [4,5]. Further, FVPR was found to be potent against viruses that have shown resistance against conventional drugs like oseltamivir and amantadine [6]. The current global health crisis of SARS COVID-19 has necessitated the exploratory usage of many re-purposed potential drug systems including FVPR. FVPR is a synthetic derivative of pyrazinamide with a marked activity towards RNA-based virus. In one of the comprehensive literature scrutiny that covered over 2600 studies by Ahmed Wadaa-Alla et al., both FVPR and HCQ demonstrated effectiveness in clearing the viral load, shortening the recovery time, and improving pneumonia [7]. The study also envisaged that FVPR and Remdesivir stand better chances as COVID-19 drugs [8] with the FVPR showing a hal-maximal response of 61.88 μM [9].

FVPR shows keto-enol tautomerism via an intramolecular proton transfer demonstrating the switching of structures between a ketone form and an alcohol form. The proton transfer is bound to cause changes in the structural and electronic properties thereby affecting the biological activities. DFT studies by L. Antonov showed that FVPR is present predominantly in the enol form in the neutral state. However, the predominant structure switches to the keto form in an acidic medium as the carboxamide group easily gets protonated [10].

Upon administration, FVPR gets converted into FVPR-RMP (favipiravir ribofuranosyl-5-monophosphate) derivative by phosphoribosylation by an enzyme [11] and this is later metabolized to the active form of FVPR-RTP (favipiravir-ribofuranosyl triphosphate) as seen in Fig. 1. While the FVPR-RMP showed mild inhibitory action, FVPR-RTP showed antiviral effects on influenza viruses by having marked inhibition towards the RNA-dependent RNA polymerase (RdRp) [12].

As FVPR is metabolized by the enzyme aldehyde oxidase and is not influenced by the cytochrome isoenzymes, it is expected to show minimum drug interactions [13]. Further, the cardiovascular side effects of FVPR are assessed to be minimum [14]. Even though FVPR appears to be relatively safer without many serious adverse effects, there is a possibility of altered serum urate levels in patients. Also, certain aspects such as teratogenic implications and altered QTc intervals etc need to be assessed further for the long-term usage of FVPR [15]. It is observed that there is a dearth of clinical safety data in the literature for the use of FVPR in Covid-19 treatment.

Drug impurities are compounds that are formed during synthesis and formulation and stay remain active along with the 'active pharmaceutical ingredients'. They might also form during storage by

* Corresponding author.
E-mail address: s_anilkumar@blr.amrita.edu (S. Anil Kumar).

https://doi.org/10.1016/j.comptc.2021.113375
Received 13 May 2021; Received in revised form 5 July 2021; Accepted 7 July 2021
Available online 17 July 2021
2210-271X/

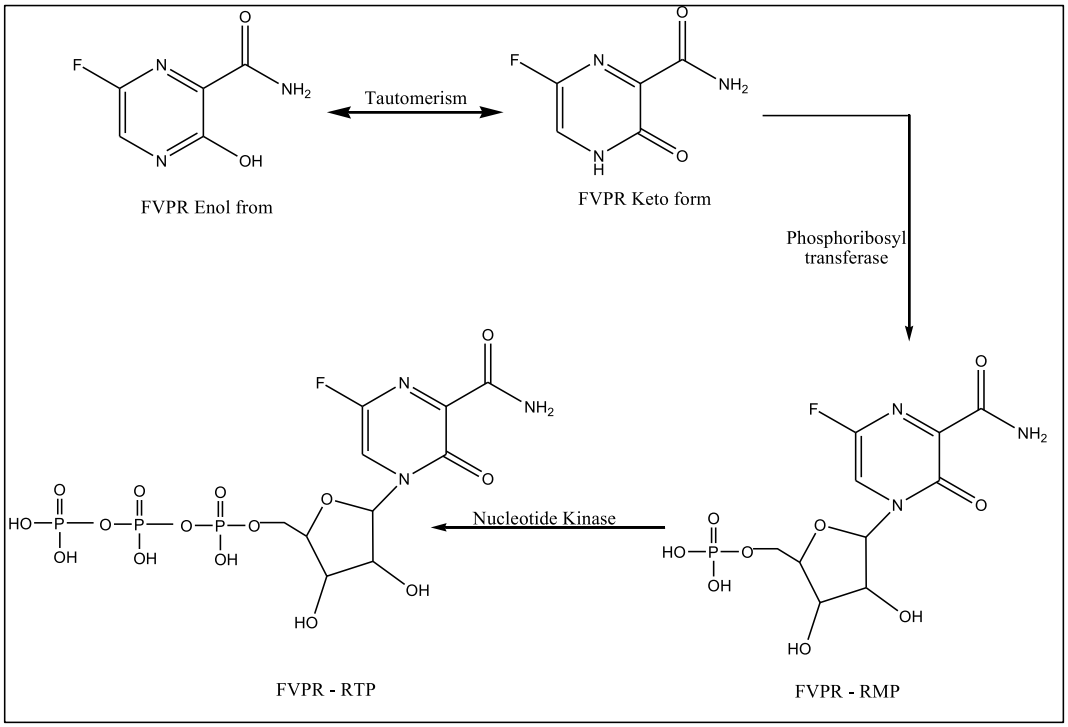

Fig. 1. Phosphoribosylation of FVPR into FVPR-RTP

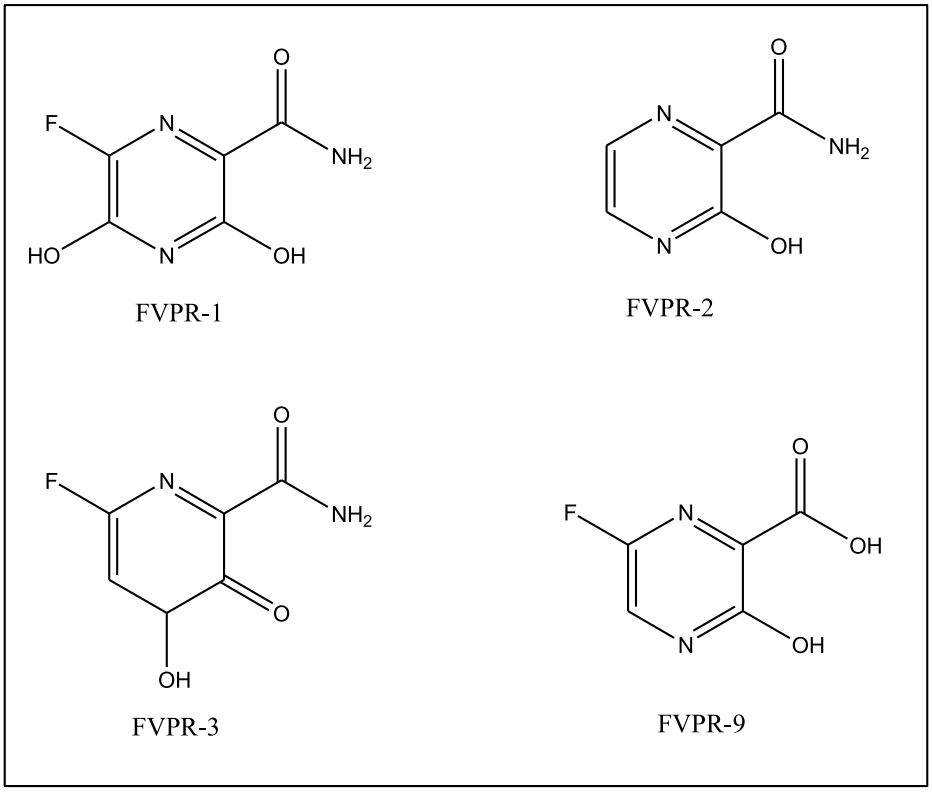

Fig. 2. Structure of FVPR-1, FVPR-2, FVPR-3 and FVPR-9.

decomposition. The term impurity often assumes a negative connotation due to its possible harmful impacts on the safety and efficacy of the drugs. Regulatory bodies stipulate that all the impurities above the critical concentration levels must be detected, qualified and reported. However, it has been observed that at times the drug impurities can be useful as their structural and clinical exploration might lead us to better drug molecules. Especially, during pressing situations such as a pandemic, they offer a plethora of lead molecules to work upon in pursuit of novel and efficient medication. 6-flouro-3,5-dihydroxypyrazine-2-carboxamide (FVPR-1), 3-hydroxypyrazine-2-carboxamide

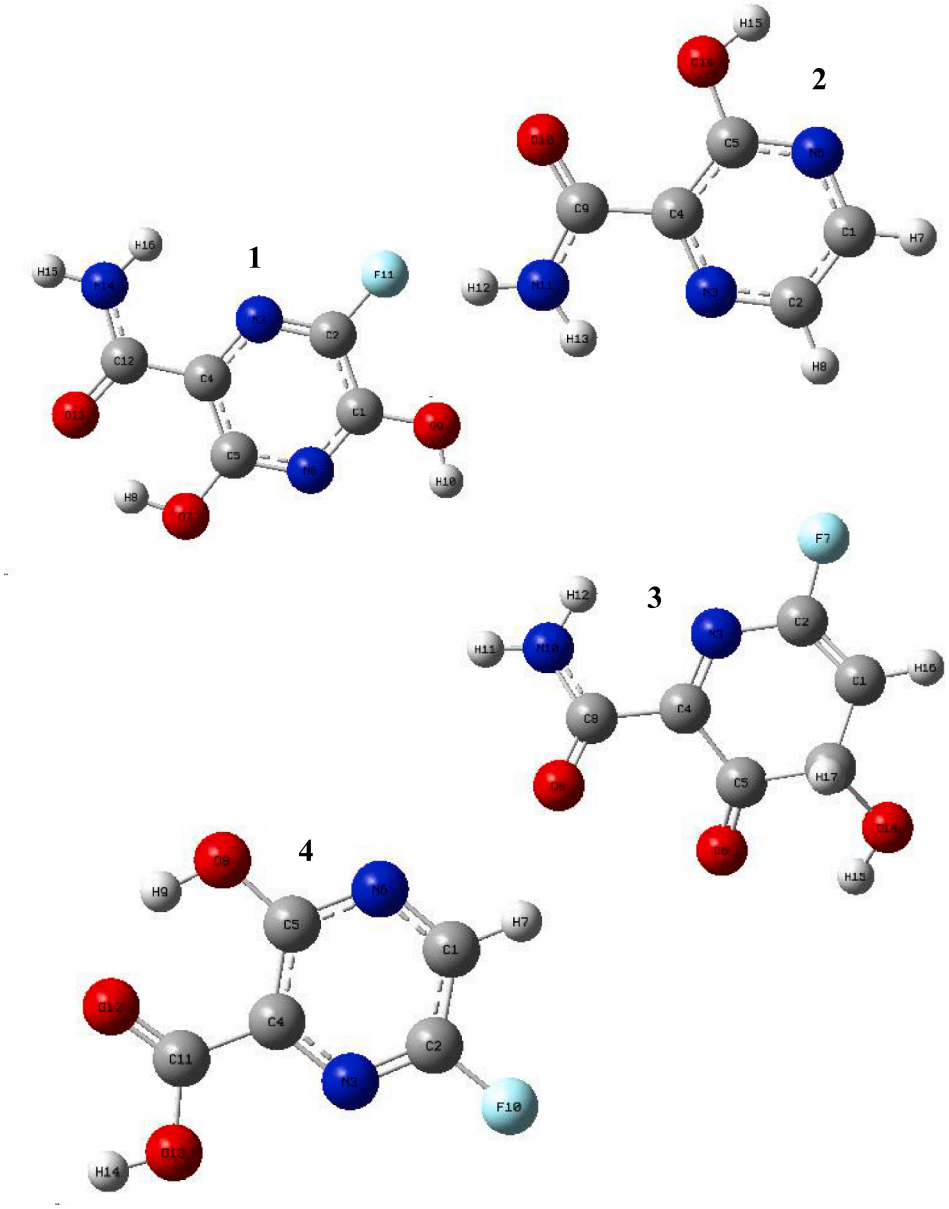

Fig. 3. Optimized geometries of [1] FVPR-1; [2] FVPR-2; [3] FVPR-3 and [4] FVPR-9 computed using DFT at B3LYP 6-311g.

Table 1
Major optimization parameters.

Parameters	FAVPR-1	FAPR-2	FAVPR-9	FAVPR-9
Global minimum energy (a.u.)	−682.7	−508.2	−666.6	−627.3
Polarizability	84.07	76.66	84.57	74.01
Dipole moment (D)	1.81	4.6	2.5	1.62
Total Thermal energy (Kcal/mol)	71.6	73.1	78.2	59.8
Heat Capacity (cal/mol·K)	37.0	30.6	39.2	31.9
Entropy (cal/mol·K)	95.7	89.2	101.5	91.1

(FVPR-2), 6-fouro-4-hydroxy-3-oxo-3,4-dihydroxypyridine-2-carboxamide (FVPR-3) and 6-flouro-3-hydroxypyrazine-2-carboxamide (FVPR-9) are process-related impurities of FVPR.

In the present study, the four impurity molecules of FVPR namely FVPR-1, FVPR-2, FVPR-3 and FVPR-9 (Fig. 2) are subjected to structural, spectral and physiochemical studies computationally to assess the drug-likeness and medicinal chemistry friendliness for potential use in antiviral treatments including COVID-19. Among the impurity molecules studied, FVPR-1, also known as hydroxyl favipiravir (T-705M1), is an established metabolite of FVPR [16]. Though FVPR-1 will be in its inactive state, its presence in plasma may lead to elevated uric acid concentration in blood [17] leading to hyperuricemia especially in patients with renal complications. Another impurity molecule FVPR-2, often designated as compound T-1105, has been explored for its potential application in antiviral treatments by Toyama Chemical Co., Ltd [18]. In another study [19], FVPR-2 was found to be effective against Zika virus replication. Further, Hutching et al [20] demonstrated that the favipiravir-ribonucleoside complex which plays a crucial role in the drug action is not very stable and easily gets decomposed by the nucleophilic displacement of Fluorine by the hydroxyl group. On the contrary, the non-fluorine analog of favipiravir, namely FAVPR-2 (T-1105) will form its ribonucleoside complex which is more stable in the given circumstances. Studies also revealed that FAVPR-2 could be a more potent antiviral drug for inhibiting influenza viruses [21].

Table 2
Calculated net charges by Mulliken Population Method and Natural Bond orbital analysis.

Atom	Natural Charge	Mulliken Charge	Atom	Natural Charge	Mulliken Charge
FVPR-1			**FVPR-3**		
C1	0.46375	0.333	C1	−0.20608	−0.118
C2	0.51487	0.407	C2	0.51844	0.424
N3	−0.42895	−0.327	N3	−0.42692	−0.339
C4	−0.02231	−0.131	C4	0.13602	0.028
C5	0.52846	0.492	C5	0.47179	0.235
N6	−0.48407	−0.321	O6	−0.47636	−0.293
O7	−0.63449	−0.543	F7	−0.33973	−0.302
H8	0.50318	0.408	**C8**	**0.59434**	**0.576**
O9	−0.63103	−0.546	O9	−0.56723	−0.372
H10	0.48931	0.401	**N10**	**−0.76237**	**−0.765**
F11	−0.32669	−0.287	H11	0.39996	0.346
C12	**0.62122**	**0.664**	H12	0.40834	0.36
O13	−0.6661	−0.491	C13	0.02073	−0.055
N14	**−0.74397**	**−0.772**	O14	−0.71355	−0.591
H15	0.40314	0.35	H15	0.47079	0.39
H16	0.41367	0.366	H16	0.24459	0.228
FVPR-2			H17	0.22726	0.247
C1	0.03344	−0.021	**FVPR-9**		
C2	−0.01818	0.027	C1	0.00972	−0.041
N3	−0.4278	−0.364	C2	0.53124	0.385
C4	0.06044	−0.017	N3	−0.37627	−0.249
C5	0.51602	0.444	C4	−0.02205	−0.126
N6	−0.48052	−0.358	C5	0.51546	0.485
H7	0.20508	0.194	N6	−0.4053	−0.278
H8	0.20502	0.188	H7	0.22095	0.222
C9	**0.60472**	**0.573**	O8	−0.62947	−0.536
O10	−0.58266	−0.377	H9	0.50137	0.407
N11	**−0.7762**	**−0.781**	F10	−0.33569	−0.298
H12	0.39437	0.336	**C11**	**0.75715**	**0.579**
H13	0.40855	0.351	O12	−0.62702	−0.435
O14	−0.61949	−0.521	**O13**	**−0.62933**	**−0.519**
H15	0.47721	0.38	H14	0.48924	0.404

2. Materials and Methods

2.1. DFT Calculations

Gaussian 09 software package [22] has been used for the computational modeling to yield the optimized structures, geometrical parameters, vibrational frequencies, frontier orbital and Mulliken charge analysis at suitable basis sets. The input for the geometry optimization was constructed and the results were interpreted using the graphical interface GaussView 6.0.

2.2. ADME Studies

The ADME properties including absorption, distribution, metabolism, and excretion were evaluated with the help of the SwissADME web tool [23,24]. The graphical output of the programme namely the bioavailability radar has been utilized for forecasting important physiochemical parameters which determine the preliminary appropriateness of the lead molecule for drug development.

3. Results and Discussions

3.1. Structural optimizations

The most optimized structures corresponding to the global minimum energy states were visualized using DFT at the basis set B3LYP/6-311 and the same have been presented in Fig. 3 with atom labeling. The global minimum energies of FVPR-1, FVPR-2, FVPR-3 and FVPR-9 are computed at −682.7, −508.2, −666.6 and −627.3 a.u. respectively indicating the most stable states both thermally and dynamically [25].

The summary of major optimization parameters computed is appended in Table 1. The parameters such as global minimum energy and polarizability are useful indicators in the prospective docking studies while the dipole moment of the molecules envisages drug-receptor interactions [26].

The polarizability provides the overall sum of partial charge distribution across the atoms and the dipole moment is the product of the sum charges and the distance between them in molecules. The results indicated that FVPR-2 has a relatively very high dipole moment of 4.6D, whereas the other three compounds have relatively lower values. A higher dipole moment generally indicates the higher intramolecular charge-transfer interactions. This also favors higher interactions with polar solvents, enhancing their solubility in biological systems [27]. The polarizability and dipole moment indices of the systems have a fundamental relationship with the individual atomic charges, and this can be further corroborated by performing the Natural bond orbitals (NBO) analysis. The NBO analysis provides an understanding of the charge-transfer interactions of molecules [28]. Another parameter that describes the electronic charge distributions in molecules is the Mulliken charge. In the Mulliken charge analysis, the sites with maximum negative charges will undergo electrophilic attack and the sites with maximum positive charges will be more prone to nucleophilic attack.

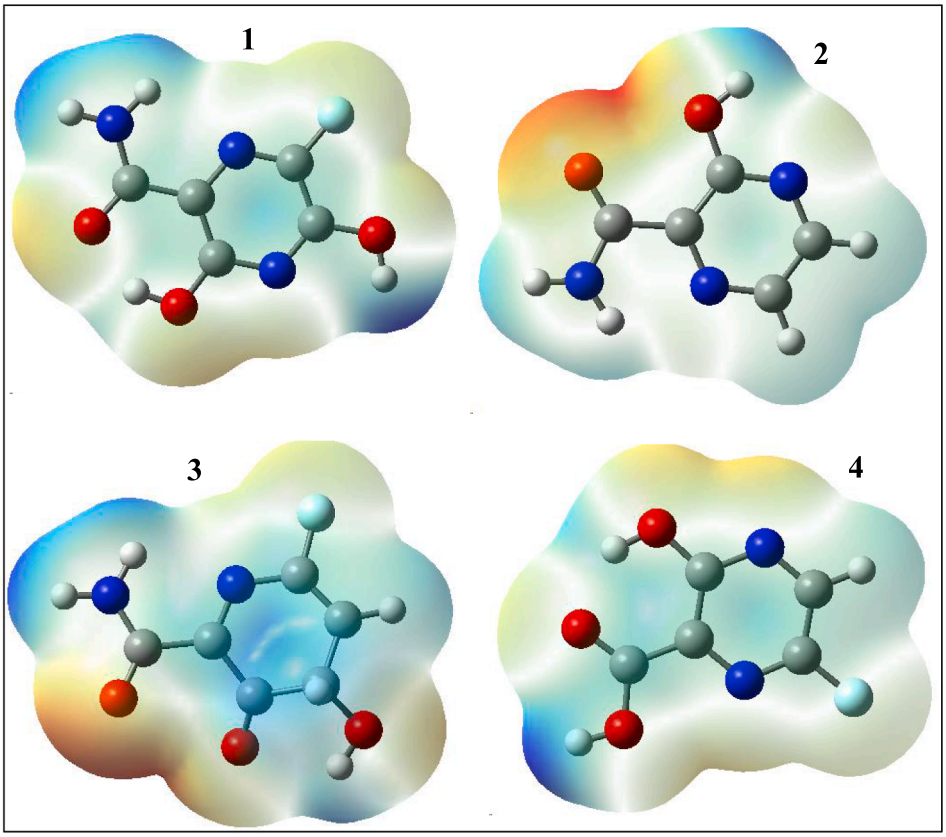

Fig. 4. MEP plots of [1] FVPR-1; [2] FVPR-2; [3] FVPR-3 and[4] FVPR-9.

Table 3
The global reactivity parameters of FVPR-1, FVPR-2, FVPR-3, and FVPR-9.

Parameter	FVPR-1	FVPR-2	FVPR-3	FVPR-9
E_{HOMO} (eV)	−7.338	−6.858	−7.397	−7.824
$E_{HOMO}-1$ (eV)	−7.973	−7.278	−7.908	−8.066
E_{LUMO} (eV)	−2.656	−2.407	−4.046	−3.280
$E_{LUMO}+1$ (eV)	−1.463	−1.316	−1.668	−1.702
ΔE (eV)	4.682	4.451	3.351	4.544
Ionization energy (I)	7.338	6.858	7.397	7.824
Electron affinity (A)	2.656	2.407	4.046	3.280
Global hardness (η)	2.341	2.225	1.675	2.272
Global softness (S)	0.214	0.225	0.298	0.220
Absolute electro negativity (χ)	4.977	4.633	5.722	5.552
Chemical potential (μ)	−4.977	−4.633	−5.722	−5.552
Electrophilicity (ω)	5.291	4.822	9.771	9.398
Maximum charge transfer index (ΔN_{max})	2.126	2.082	3.416	2.443

The natural charges computed by the NBO analysis and Mulliken charges of FVPR-1, FVPR-2, FVPR-3, and FVPR-9 are appended in Table 2.

The computed results demonstrate that the most positive site in all the four compounds is the carboxamide carbon (0.62122 at C12 in FVPR-1; 0.60472 at C9 in FVPR-2; 0.59434 at C8 in FVPR-3 and 0.75715 at C11 in FVPR-9) and hence will be liable for an attack by the nucleophiles. Conversely, the most negative site in FVPR-1, FVPR-2, and FVPR-3 was found at the amino nitrogen (−0.74397 at N14, −0.7762 at N11 and −0.76237 at N10 respectively) while the same in FVPR-9 was seen at the hydroxyl oxygen of the carboxylic acid group (−0.62933 at O13). These sites will be susceptible to electrophilic attacks. The proclivity of intermolecular interactions of the drug systems with the receptors can also be studied with the help of electrostatic potential maps (MEP) derived from the DFT computations. These plots are generated by plotting the electrostatic potentials onto the fixed electronic density surfaces [28]. The MEP is a useful tool in assessing the reactivity of drug systems towards electrophilic and nucleophilic attacks [29] by using a color gradient in which the most electropositive and negative sites are represented in blue and red respectively. The MEP plots visualized computationally are presented in Fig. 4.

The MEP plots show that the hydrogen atoms attached to the amino group and the carbonyl oxygen are more susceptible to nucleophilic and electrophilic attacks, respectively.

3.2. Frontier orbital analysis

The Highest Occupied (HOMO) and Lowest Unoccupied (LUMO) Molecular Orbitals, commonly known as the frontier orbitals, often provide valuable information regarding the electron-donating and electron-gaining tendencies of the drug molecules. This will in turn, help us to assess the drug-receptor biochemical interactions, thermodynamical stability and chemical reactivity [30,31].

The HOMO-LUMO energy gap further reveals the scope of electron excitation between the highest occupied and lowest unoccupied orbitals, thus describing the overall stability. The frontier orbitals of the lead

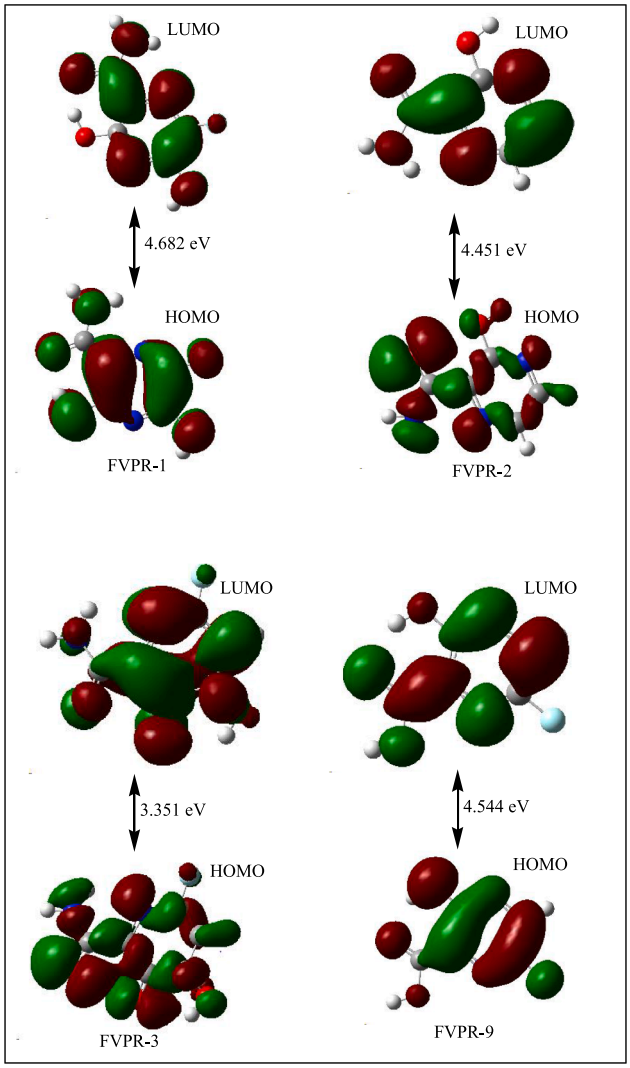

Fig. 5. HOMO-LUMO plots of FVPR-1, FVPR-2, FVPR-3, and FVPR-9.

molecules visualized via DFT studies can be used to obtain several useful global reactivity parameters namely, the chemical potential, absolute electroegativity, global softness, global hardness, electrophilicity, etc. These descriptors are calculated using the following Eqs. (1)–(8).

$$\text{Ionization potential (I)} = -E_{HOMO} \quad (1)$$

$$\text{Electron affinity (A)} = -E_{LUMO} \quad (2)$$

$$\text{Absolute electronegativity } (\chi) = \frac{I + A}{2} \quad (3)$$

$$\text{Chemical potential } (\mu) = -\chi \quad (4)$$

$$\text{Global hardness } (\eta) = \frac{E_{LUMO} - E_{HOMO}}{2} \quad (5)$$

$$\text{Global softness (S)} = \frac{1}{2\eta} \quad (6)$$

$$\text{Electrophilicity } (\omega) = \frac{\mu^2}{2\eta} \quad (7)$$

$$\text{Maximum charge transfer index } (\Delta N_{max}) = -\frac{\mu}{\eta} \quad (8)$$

The results in Table 3 showed that FVPR-2 has the highest HOMO energy and FVPR-3 has the lowest LUMO energy making them the most nucleophilic and electrophilic systems, respectively. The HOMO-LUMO energy difference of FVPR-1, FVPR-2 and FVPR-9 are relatively higher and comparable while that of FVPR-3 is relatively smaller at 3.351 eV. In general, a relatively higher ΔE represents higher stability and a lower ΔE indicates more chemical reactivity.

FVPR-9 and FVPR-2 demonstrated the highest and lowest ionization energies respectively. It is noted that systems with a high Electrophilicity index (ω) will be less reactive and act as electrophiles. Going by this thumb rule, FVPR-3 will be more stable and nucleophilic in nature. Conversely, FVPR-2 will be more reactive and electrophilic during drug-receptor interactions. Further FVPR-2 shows the lowest absolute electronegativity (χ) and thereby making it the most basic of the lot. This could be an important marker that governs the intracellular interactions of the drug.

The HOMO and LUMO contour plots of the molecules are visualized using DFT are presented below (Fig. 5). These plots have red and blue regions representing the negative and positive phases of the wave function, respectively. In FVAPR-1, the HOMO is populated throughout the molecule except on the pyrazine nitrogens. The hydroxyl oxygen, the O and N on the carboxamide and the fluorine atoms contribute to the HOMO. The pyrazine nitrogens, O and N on the carboxamide, mainly contribute to the LUMO with no population over the fluorine atom.

In FVPR-2, the HOMO has contributions from the carbonyl oxygen, pyrazine nitrogens and hydroxyl oxygen atoms. The LUMO is highly localized over the pyrazine nitrogens and the carboxamide moiety with no population over the OH groups. In FVPR-3, the HOMO is mainly due to the O and N of carboxamide and pyrazine nitrogens whereas the LUMO is mainly due to carbonyl oxygen attached to the ring and pyrazine nitrogens. Again, there is no involvement from the fluorine atoms. In FVPR-9, the HOMO contributions involve the pyrazine nitrogen hydroxyl oxygen and fluorine atoms. The LUMO is primarily due to the COOH and the ring with no population over the fluorine atom.

Of the molecules studied, FVPR-1, FVPR-2, and FVPR-9 showed comparable HOMO-LUMO band gap with FVPR-3 showing a relatively lower value at 3.351 eV. It is attributed to the smaller aromatic system in FVPR-3. The comparatively shorter energy gaps of the molecules suggest the feasibility of electron transfer and increased chemical reactivity. The HOMO-LUMO energies were also assessed by using the Density of States (DOS) plots in which the occupied and virtual orbitals are illustrated (Fig. 6). The HOMO-LUMO distribution along with the electrostatic potential plots often provide suggestive inputs for the potential docking studies as the HOMO of the ligand molecule is expected to bind with the LUMO of the receptor molecule. Therefore, it is envisaged that higher HOMO energy of the lead molecule favors docking [32].

3.3. Geometrical Parameters

Geometrical parameters including the bond lengths and bond angles of FVPR-1, FVPR-2, FVPR-3, and FVPR-9 compared against the experimental values [33]. In general, the computed and experimental results showed necessary consilience (Table 4). It is expected that all three molecules except FVPR-3 show keto-enol tautomerism. The noticeable reduction in the bond lengths involving the OH group is attributed to the possibilities of hydrogen bonding involving these atoms. The same trend

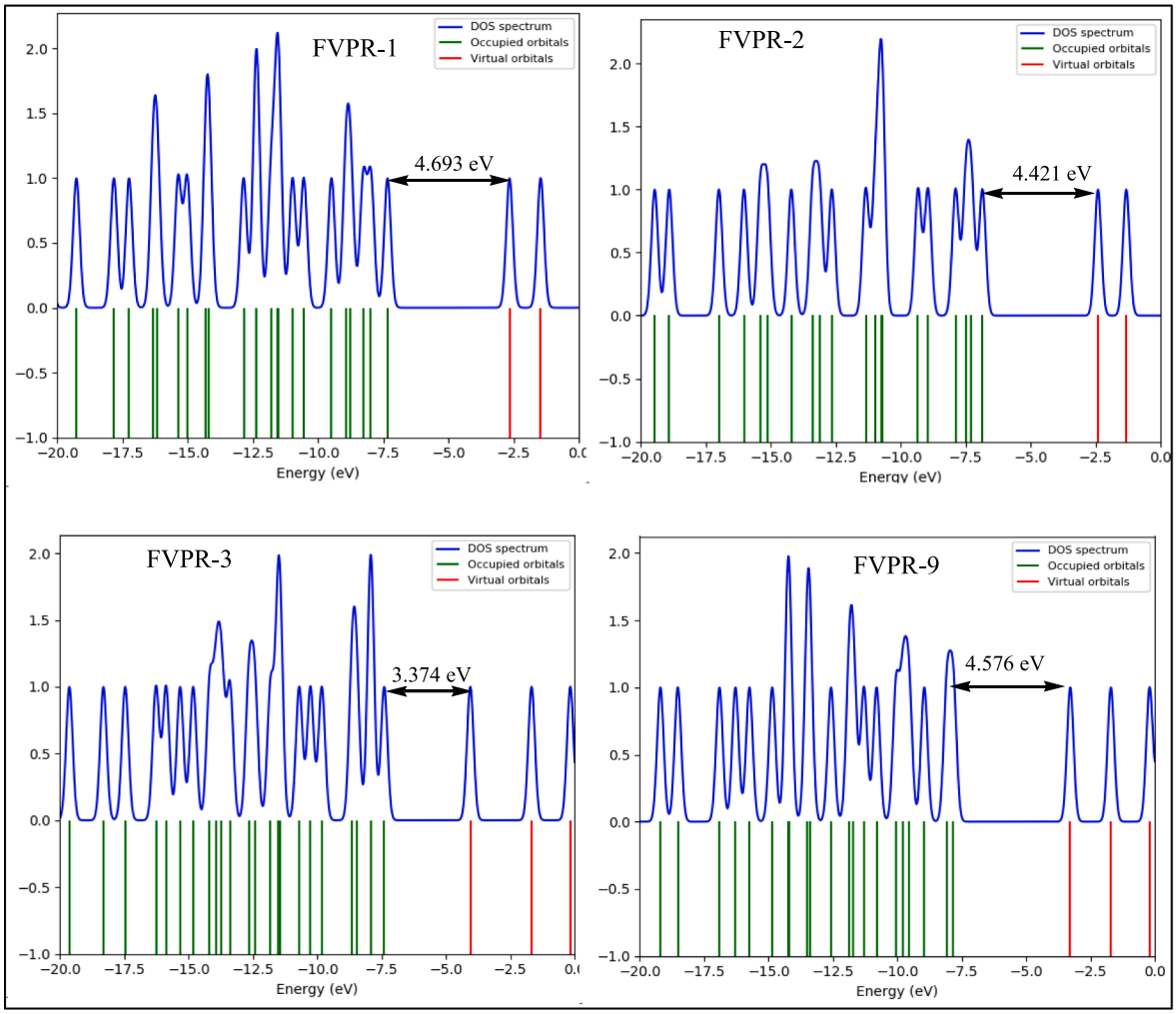

Fig. 6. DOS plots of FVPR-1, FVPR-2, FVPR-3, and FVPR-9.

is also noticed among the N—H bond lengths of carboxamide moieties, again owing to the hydrogen bonding. Intramolecular hydrogen bonding is visualized at O7—H8—O13 (2.727 Å) for FVPR-1 and at O8—H9—O12 (2.787 Å) for FVPR-9. All the molecules are capable of intermolecular hydrogen bonding that involves the NH_2. The compounds FVPR-1, FVPR-2 and FVPR-9 are structurally planar including the fluorine as evident from their torsional angles whereas, in FVPR-3 the carboxamide moiety is placed at a dihedral angle of 20 Å.

3.4. FTIR Studies

Even though FTIR data are often overlooked during the structural and geometrical optimization, it can substantiate the optimized structure corresponding to the global minimum energy by having all positive force constant values. All the characteristic wave numbers are identified and present in the consolidated FTIR plot (Fig. 7). The trademark twin peaks of amino group corresponding to the asymmetric and stretching modes are computed at 3700 and 3500 cm^{-1} respectively for FVPR-1, FVPR-2, and FVPR-3. The OH stretching modes are computed at around 3600 cm^{-1} for all four compounds. In FVPR-9, the stretching vibrations involving the —OH of the carboxylic acid group are visualized at 3350 and 3640 cm^{-1} respectively. The other significant peaks such as NH2 scissoring and C═O stretching are computed at 1680 and 1630 cm^{-1} respectively. As expected, the vibrations involving C—O, C—N, C—F, N—H, C—H, O—H and the ring stretch dominate the fingerprint region.

3.5. Absorption-Distribution-Metabolism-Excretion (ADME) studies

The ADME studies are conducted computationally to evaluate the extent of absorption of the drug, its distribution in the body, various metabolic processes it undergoes, and finally the elimination of the drugs from the body. These parameters also give us a preclinical assessment of the overall toxicity of the lead molecules. ADME-based filtering studies help us to handpick the best druglike molecules and also help to minimize potential failures at an advanced stage, by avoiding the unsuitable candidates initially [34,35]. For better pharmacological efficacy, the selected drugs are expected to present inside the body in the right quantity for the right duration of time before getting excreted. Useful parameters namely flexibility, lipophilicity, size, polarity, solubility and saturation and their functional limits are computed and presented using the bioavailability radar (Fig. 8) function of the program. Further, important clinical aspects such as gastrointestinal absorption (HIA), blood-brain-barrier (BBB) permeability,

Table 4
Geometrical parameters of FVPR-1, FVPR-2, FVPR-3, and FVPR-9 compared against the experimental results.

FVPR-1		FVPR-2		FVPR-3		FVPR-9		Exptl.
C1—C2	1.41	C1—N6	1.35	C1—C2	1.34	C1—C2	1.40	1.39
C1—N6	1.33	C1—C2	1.39	C1—C13	1.50	C1—N6	1.34	1.31
C1—O9	1.36	–	–	–	–	–	–	1.33
C2—N3	1.30	N6—C5	1.35	C2—N3	1.39	C2—N3	1.31	1.30
C2—F11	1.38			C2—F7	1.39	C2—F10	1.39	1.34
N3—C4	1.36	C5—C4	1.41	N3—C4	1.30	N3—C4	1.36	1.34
C4—C5	1.41	C4—N3	1.30	C4—C5	1.50	C4—C5	1.42	1.40
C4—C12	1.47	C4—C9	1.50	C4—C8	1.50	C4—C11	1.46	1.48
C5—N6	1.35	N3—C2	1.39	C5—C13	1.52	C5—N6	1.35	1.31
C5—O7	1.35	–	–	C5—O6	1.24	C5—O8	1.35	1.33
O7—H8	1.00	–	–	–	–	O8—H9	0.99	0.82
O9—H10	0.98	O14—H15	0.98	O14—H15	0.98	O13—H14	0.98	0.82
C12—O13	1.27	C9—O10	1.25	C8—O9	1.25	C11—O12	1.25	1.24
C12—N14	1.35	C9—N11	1.36	C8—N10	1.36	C11—N13	1.35	1.32
N14—H15	1.00	N11—H12	1.00	N10—H11	1.01	–	–	0.86
						O13—H14	0.98	–
N14—H16	1.01	N11—H13	1.01	N10—H12	1.01			0.86
Bond angles								
C2—C1—N6	120.57	C2—C1—N6	120.86	C2—C1—C13	117.89	C2—C1—N6	120.04	121.20
C1—C2—N3	121.36	C1—N6—C5	118.77	C1—C2—N3	125.68	C1—C2—N3	123.27	123.30
C1—C2—F11	119.98	–	–	C1—C2—F7	121.70	C1—C2—F10	118.95	119.90
N3—C2—F11	118.66	–	–	N3—C2—F7	112.62	N3—C2—F10	117.78	116.80
C2—N3—C4	119.18	C4—C5—N6	121.22	C2—N3—C4	120.85	C2—N3—C4	117.57	116.30
N3—C4—C5	119.92	N3—C4—C5	118.82	N3—C4—C5	119.82	N3—C4—C5	120.38	121.40
N3—C4—C12	119.04	C5—C4—C9	124.75	N3—C4—C8	118.51	N3—C4—C11	119.59	118.00
C5—C4—C12	121.04	N3—C4—C9	116.43	C5—C4—C8	121.63	C5—C4—C11	120.03	120.70
C4—C5—N6	120.00	C2—N3—C4	120.06	C4—C5—C13	115.09	C4—C5—N6	120.43	120.80
C4—C5—O7	122.83	–	–	C4—C5—O6	124.50	C4—C5—O8	123.75	123.50
N6—C5—O7	117.16	–	–	O6—C5—C13	120.33	N6—C5—O8	115.82	115.60
C1—N6—C5	118.97	C1—C2—N3	120.26	C1—C13—C5	112.40	C1—N6—C5	118.30	117.00
C5—O7—H8	108.75	–	–	–	–	C5—O8—H9	110.49	109.50
C1—O9—H10	110.08	–	–	–	–	–	–	–
C4—C12—O13	120.03	C4—C9—O10	123.11	C4—C8—O9	121.08	C4—C11—O12	122.25	119.70
C4—C12—N14	117.08	C4—C9—N11	113.61	C4—C8—N10	114.47	C4—C11—O13	115.79	117.30
O13—C12—N14	122.89	O10—C9—N11	123.28	O9—C8—N10	124.41	O12—C11—O13	121.95	123.10
C12—N14—H15	119.29	C9—N11—H13	120.00	C8—N10—H11	118.82	C11—O13—H14	110.62	120.00
C12—N14—H16	120.00	C9—N11—H12	118.56	C8—N10—H12	120.57			120.00
H15—N14—H16	120.71	H12N11H13	121.43	H11—N10—H12	120.38	C11—O13—H14	110.62	120.00

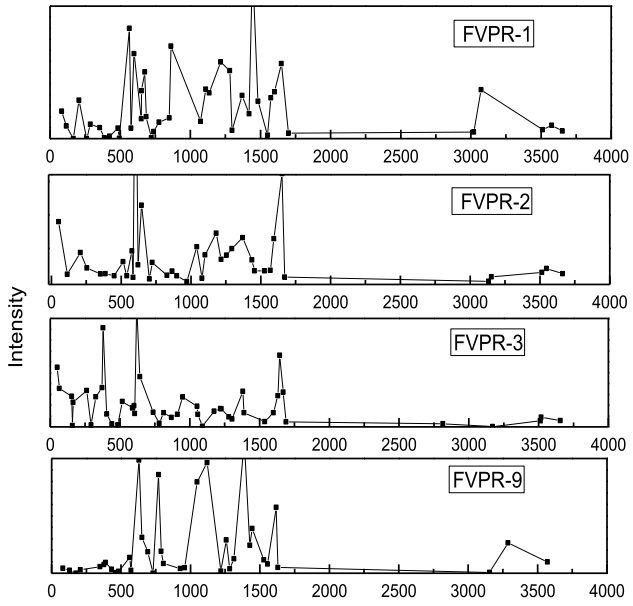

Fig. 7. Consolidated FTIR spectra of FVPR-1, FVPR-2, FVPR-3, and FVPR-9.

topological polar surface area (TPSA) etc. of the compounds were also derived (Table 5).

The results showed that all four compounds show more or less similar physiochemical properties as compared to Favipiravir. All the compounds are free from any Lipinski violations, suggesting good drug-like properties. Among the compounds studied, FVPR-1 has 6 hydrogen bond acceptors and 3 donors indicating more reactivity than others with the receptor systems. All the compounds showed an either negative or very low value of logP making them highly hydrophilic and almost non-toxic. The topological polar surface area of all the compounds is close to 90 $[Å]^2$ which is the threshold value for being a blood-brain-barrier permeant. Again FVPR-1showed relatively higher values of TPSA than others owing to the presence of an additional polar hydroxyl group. In general, an elevated TPSA and a very low logP demonstrate ensure superior bioavailability of the systems upon oral administration. The molar refractivity which is the measure of the overall polarity of molecules is in the range of 30.9 to 39.7 which is slightly below the optimal cut-off value of 40. The cytochrome inhibitory actions of all the lead molecules are comparable to that of the parent drug.

The SwissADME tool also provides a graphics output called the BOILED-Egg plot which outlines the gastrointestinal or CNS absorption rates of the potential drugs. In the BOILED-Egg plot, the molecules that are present in the egg's white will undergo GI absorption, while those in the yolk would be more prone to CNS absorption (Fig. 9). It is also noted

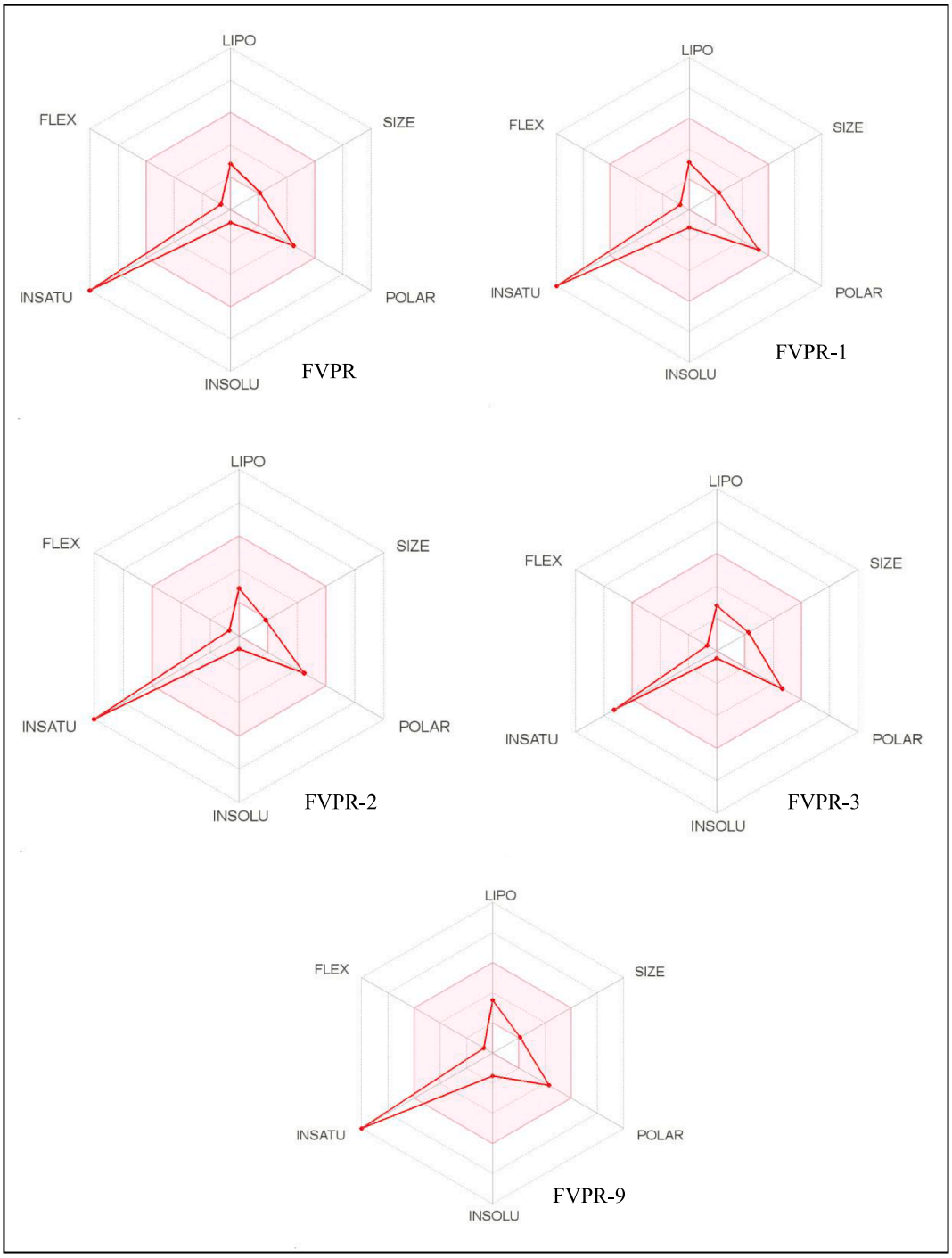

Fig. 8. Bio-availability radars of the metabolites and parent drugs

Table 5
The physiochemical properties of lead molecules compared against the parent molecules.

Molecule	FVPR	FVPR-1	FVPR-2	FVPR-3	FVPR-9
Molecular weight (g)	157.1	173.1	139.11	172.11	158.09
No. of heavy atoms	11	12	10	12	11
No of rotatable bonds	1	1	1	1	1
No. of H-bond acceptors	4	6	4	5	6
No. of H-bond donors	2	3	2	2	2
Molar refractivity	32.91	34.13	32.15	39.7	30.97
TPSA,([Å]^2	88.84	109.33	89.1	92.75	83.31
Consensus Log P	−0.27	−0.42	−0.6	−0.71	0.19
ESOL Log S	−0.8	−1.17	−0.78	−0.46	−1.54
Solubility	Very soluble	Very soluble	Very soluble	Very soluble	Very soluble
GI absorption	High	High	High	High	High
BBB permeant	No	No	No	No	No
Pgp substrate	No	No	No	No	No
CYP1A2 inhibitor	No	No	No	No	No
CYP2C19 inhibitor	No	No	No	No	No
CYP2C9 inhibitor	No	No	No	No	No
CYP2D6 inhibitor	No	No	No	No	No
CYP3A4 inhibitor	No	No	No	No	No
log Kp (cm/s)	−7.66	−7.41	−7.49	−7.78	−6.83
Lipinski #violations	0	0	0	0	0
Bioavailability Score	0.55	0.55	0.55	0.55	0.56
PAINS #alerts	0	0	0	0	0
Brenk #alerts	0	0	0	1	0
Leadlikeness #violations	1	1	1	1	1
Synthetic Accessibility	2.08	2.3	1.77	3.38	2.12

that if the molecule is present in the grey area, they are expected to show poor GI and CNS absorption rates. The results showed that FVPR and its impurities are present in the 'white' region demonstrating good GI absorption properties. In general, all the compounds studied showed good GI absorption and poor BBB permeation suggesting almost no effect on the CNS system.

4. Conclusions

Four structurally analogous impurity molecules of FVPR are investigated computationally to reveal the structural, spectral and electronic properties. The geometrical parameters computed showed a satisfactory concordance with the experimental results. Our results showed that FVPR-2 has a relatively very high dipole moment of 4.6D indicating high probabilities of intramolecular charge transfer interactions. The most positive site (liable for nucleophilic attack) in all the four compounds is the carboxamide carbon, whereas the most negative site (liable for electrophilic attack) in FVPR-1, FVPR-2, and FVPR-3 was found at the amino nitrogen. The same for FVPR-9 was seen at the hydroxyl oxygen of the carboxylic acid group. The MEP plots further revealed that the hydrogen atoms attached to the amino group and the carbonyl oxygen are more susceptible to nucleophilic and electrophilic attacks respectively. Further, the assessment of ADME parameters revealed that all the lead molecules possessed very low logP values indicating very minimal toxicity and hydrophilicity which are hallmarks of good drug systems. FVPR-1 has 6 hydrogen bond acceptors and 3 donors indicating more reactivity with the receptor systems and showed relatively higher values of TPSA due to the presence of an additional polar hydroxyl group.

FVPR-9 and FVPR-2 demonstrated the highest and lowest ionization energies, respectively. Going by the thumb rule of Electrophilicity index (ω), FVPR-3 will be more stable and nucleophilic while FVPR-2 will be more reactive and electrophilic in nature during drug-receptor interactions. Further FVPR-2 shows the lowest absolute electronegativity (χ) and thereby making it the most basic of the lot. This could be an important marker that governs the intracellular interactions of the drug.

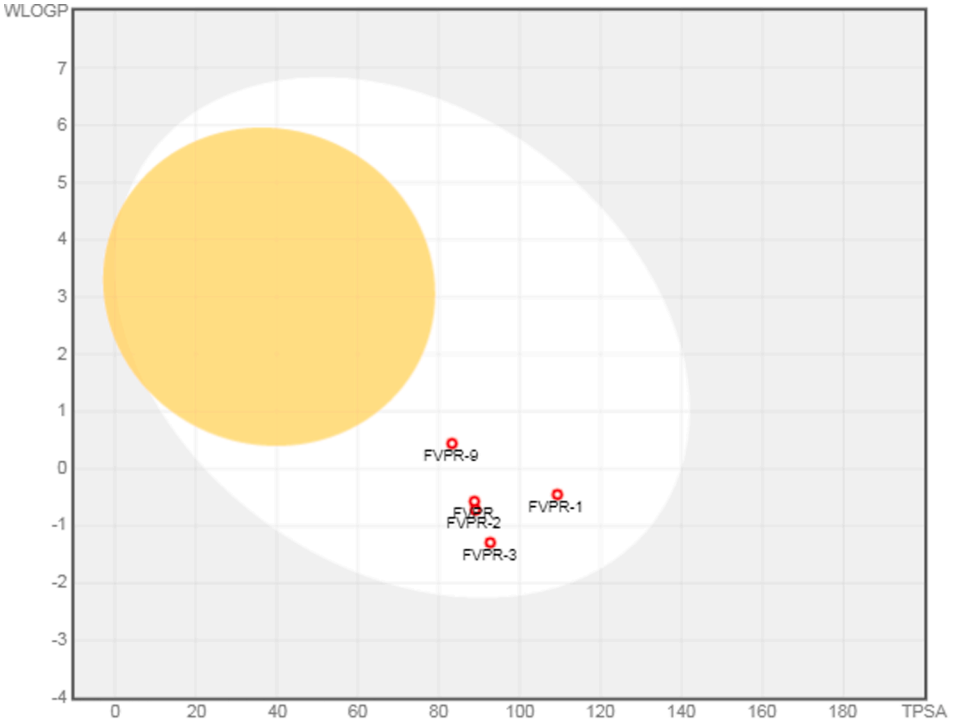

Fig. 9. BOILED-Egg plot for the metabolites and parent drug molecules.

All these listed parameters could be useful indicators in assessing binding interactions of the lead molecules with protein receptors in the potential docking studies.

CRediT authorship contribution statement

S. Anil Kumar: Conceptualization, Methodology, Software, Data curation, Writing – original draft. **B.L. Bhaskar:** Visualization, Supervision, Writing - review & editing.

Declaration of Competing Interest

The authors declare that they have no known competing financial interests or personal relationships that could have appeared to influence the work reported in this paper.

References

[1] U. Agrawal, R. Raju, Z.F. Udwadia, Favipiravir: A new and emerging antiviral option in COVID-19, Med. J. Armed Forces, India 76 (4) (2020) 370–376.
[2] Y. Furuta, K. Takahashi, M. Kuno-Maekawa, H. Sangawa, et al., Mechanism of action of T-705 against influenza virus, Antimicrob. Agents Chemother. 49 (2005) 981–986.
[3] De Clercq, New nucleoside analogues for the treatment of hemorrhagic fever virus infections, Chem. Asian J. 14 (2019) 3962–3968.
[4] M. Kiso, K. Takahashi, Y. Sakai-Tagawa, K. Shinya, et al., T-705 (favipiravir) activity against lethal H5N1 influenza A viruses, Proc. Natl. Acad. Sci. U. S. A. 107 (2010) 882–887.
[5] R.W. Sidwell, D.L. Barnard, C.W. Day, D.F. Smee, et al., Efficacy of orally administered T-705 on lethal avian influenza A (H5N1) virus infections in mice, Antimicrob. Agents Chemother. 51 (2017) 845–851.
[6] K. Sleeman, V.P. Mishin, V.M. Deyde, Y. Furuta, et al., In-vitro antiviral activity of favipiravir (T-705) against drugresistant influenza and 2009 A(H1N1) viruses, Antimicrob. Agents Chemother. 2010 (54) (2010) 2517–2524.
[7] A. Wadaa-Allah, M.S. Emhamed, M.A. Sadeq, N.B.H. Dahman, et al., Efficacy of the current investigational drugs for the treatment of COVID-19: a scoping review, Ann. Med. 53 (2021) 318–334.
[8] Q. Cai, M. Yang, D. Liu, J. Chen, et al., Experimental Treatment with Favipiravir for COVID-19: An Open-Label Control Study, Engineering 6 (10) (2020) 1192–1198.
[9] M. Wang, R. Cao, L. Zhang, X. Yang, et al., Remdesivir and chloroquine effectively inhibit the recently emerged novel coronavirus (2019-nCoV) in vitro, Cell Res 30 (2020) 269–271.
[10] L. Antonov, Favipiravir tautomerism: a theoretical insight, Theor. Chem. Acc. 139 (8) (2020) 145.
[11] Y. Furuta, K. Takahashi, M. Kuno-Maekawa, H. Sangawa, et al., Mechanism of Action of T-705 against Influenza Virus, Antimicrob Agents Chemother. 49 (3) (2005) 981–986.
[12] D. Tian, Y. Liu, C. Liang, L. Xin, et al., An update review of emerging small-molecule therapeutic options for COVID-19, Biomed. Pharmacother. 137 (2021), 111313.
[13] B.B. Gowen, E.J. Sefing, J.B. Westover, D.F. Smee, et al., Alterations in favipiravir (T-705) pharmacokinetics and biodistribution in a hamster model of viral hemorrhagic fever, Antivir Res. 121 (2015) 132–137.
[14] P. Chinello, N. Petrosillo, S. Pittalis, G. Biava, et al., QTc interval prolongation during favipiravir therapy in an Ebolavirus-infected patient, PLoS Negl. Trop. Dis. 11 (12) (2017), e0006034.
[15] V. Pilkington, T. Pepperrell, A. Hill, A review of the safety of Favipiravir – a potential treatment in the COVID-19 pandemic? J. Virus Erad. 6 (2020) 45–51.
[16] C. De Savi, D.L. Hughes, L. Kvaerno, Quest for a covid-19 cure by repurposing small-molecule drugs: mechanism of action, clinical development, synthesis at scale, and outlook for supply, Org. Process Res. Dev. 24 (2020) 940–976.
[17] E. Mishima, N. Anzai, M. Miyazaki, T. Abe, Uric acid elevation by Favipiravir, an antiviral drug, Tohoku J. Exp. Med. 251 (2020) 87–90.
[18] Y. Furutaa, K. Takahashia, K. Shirakib, K. Sakamotoc, et al., T-705 (favipiravir) and related compounds: Novel broad-spectrum inhibitors of RNA viral infections, Antiviral Res. 82 (2009) 95–102.
[19] L. Cai, Y. Sun, Y. Song, L. Xu, et al., Viral polymerase inhibitors T-705 and T-1105 are potential inhibitors of Zika virus replication, Arch. Virol. 162 (2017) 2847–2853.
[20] J. Huchting, M. Winkler, H. Nasser, C. Meier, Synthesis of T-705-ribonucleoside and T-705-ribonucleotide and studies of chemical stability, Chem. Med. Chem. 12 (2017) 652–659.
[21] J. Huchting, E. Vanderlinden, M. Winkler, M. Nasser, H. Naesens, et al., Prodrugs of the phosphoribosylated forms of hydroxypyrazinecarboxamide pseudobase T-705 and its de-fluoro analogue T-1105 as potent influenza virus inhibitors, J. Med. Chem. 61 (2018) 6193–6210.
[22] M.J. Frisch, G.W. Trucks, H.B. Schlegel, Gaussian, Inc., Wallingford, CT, 2009.
[23] A. Daina, O. Michielin, V. Zoete, SwissADME: a free web tool to evaluate pharmacokinetics, drug-likeness and medicinal chemistry friendliness of small molecules, Nature Sci. Rep. 7 (42717) (2017) 1–13.
[24] A. Daina, V. Zoete, A BOILED-Egg to predict gastrointestinal absorption and brain penetration of small molecules, Chem. Med. Chem. 11 (11) (2016) 1117–1121.
[25] L. Yi, F. Zhen, S. Qian, et al., M. Electronic, thermoelectric, transport and optical properties of MoSe2/BAs van der Waals heterostructures, Results Phys. 23 (2021), 104010.
[26] E.J. Lien, Z.R. Guo, R.L. Li, et al., Use of dipole moment as a parameter in drug-receptor interaction and quantitative structure-activity relationship studies, J. Pharm. Sci. 71 (1982) 641–655.
[27] S.M.A. Rauf, P.I. Arvidsson, F. Albericio, T. Govender, et al., The effect of N-methylation of amino acids (Ac-X-OMe) on solubility and conformation: a DFT study, Org. Biomol. Chem. 13 (2015) 9993–10006.
[28] Z. Demircioglu, C.A. Kastas, O. Buyukgungor, Theoretical analysis (NBO, NPA, Mulliken Population Method) and molecular orbital studies (hardness, chemical potential, electrophilicity and Fukui function analysis) of (E)-2-((4-hydroxy-2-methylphenylimino)methyl)-3-methoxyphenol, J. Mole. Struct. 1091 (2015) 183–195.
[29] M. Hagar, H.A. Ahmed, G. Aljohani, O.A. Alhaddad, Investigation of some antiviral n-heterocycles as covid 19 drug: molecular docking and DFT calculations, Int. J. Mol. Sci. 21 (2020) 3922.
[30] S.A. Kumar, B.L. Bhaskar, Structural elucidation of antihemorrhage drug molecule Diethylammonium 2,5-dihydroxybenzene sulfonate - An insilico approach, IOP Conf. Ser.: Mater. Sci. Eng. 310 (2018), 012124.
[31] S.A. Kumar, B.L. Bhaskar, Computational and spetral studies of Nimesulide impurity D: 4Nitro 2-Phenoxy aniline, Asian J. Chem. 27 (2015) 3907–3912.
[32] G. Shanmugam, S.K. Lee, J. Jeon, Identification of potential nematicidal compounds against the pine wood nematode, bursaphelenchus xylophilus through an in silco approach, Molecules 2018 (1828) 23.
[33] L. Rhyman, M. Tursun, H.H. Abdallah, Y.S. Choong, et al., Theoretical investigation of the derivatives of favipiravir (T-705) as potential drugs for Ebola virus, Phys. Sci. Rev. 3 (2018).
[34] S.A. Kumar, B.L. Bhaskar, Spectroscopic and computational approach for the structure-property relationship of hydantoin drug impurity: 1-methyl-5,5-diphenylimidazolidine-2, 4-dione, IOP Conf. Ser. Mater. Sci. Eng. 577 (2019), 012180.
[35] S.A. Kumar, B.L. Bhaskar, Computational and spectral studies of 3, 3'-(propane-1,3-diyl)bis(7,8-dimethoxy-1,3,4,5-tetrahydro-2H-benzo[d]azepin-2-one), Heliyon 30 (5(9)) (2019) e02420.